Journal of Global Positioning Systems (*2021*)
Vol. 17, No. 1: 65-80
DOI: 10.5081/jgps.17.1.65

Journal of Global Positioning Systems
2021
© CPGPS

Performance Analysis of BDS-2, BDS-3 and GPS in Relative Positioning through Short, Medium and Long Baselines

Huizhong Zhu*, Jingfa Zhang, Jun Li, Qi Xu, YangYang Lu and **Aigong Xu**

School of Geomatics, Liaoning Technical University (LNTU), Fuxin 123000, China;

***** Correspondence author, email: zhuhuizhong@lntu.edu.cn

Abstract: BDS-3 (Beidou System 3) reached global coverage in June 2020. In comparison with BDS-2 (Beidou system 2), BDS-3 has greatly improved in terms of satellite orbits, atomic clocks and signal transmissions. BDS-3 is now being used widely in practice. This paper is focused on performance analysis of BDS-3 vs.BDS-2 and GPS. Six baselines of different lengths were selected to result in single-system multi-frequency relative positioning solutions from BDS-2, BDS-3 and GPS, respectively. The long baselines were resolved by using the random walk constraints on the residual atmospheric delay. The positioning performance of each system was analysed against the atmospheric delay error and the convergence property of the floated ambiguity resolution. The experiments showed that the convergence speed of BDS-3 was twice as fast as BDS-2, and the average convergence speed was also faster than GPS, which was increased by about 2.7%. In comparison with BDS-2, the accuracy of BDS-3 was improved by about 40%, but the accuracy was 7% lower than the GPS solution and the positioning stability of BDS-3 was also not as good as GPS.

Keywords: convergence speed; atmospheric delay constraint; carrier phase integer ambiguity; BDS-3; baseline solution

1. Introduction

The Beidou Satellite Navigation System is the third mature Global Navigation Satellite Systems (GNSS) after the Global Positioning System (GPS) and the GLObal NAvigation Satellite System (GLONASS). Beidou has been developed after a "three-step" strategy [1~4] to gradually provide users with its relevant services around the world. BDS-1 was an experimental regional satellite navigation system consisted of three geostationary satellites to serve China. BDS-2, formerly known as COMPASS, was completed in 2012. It included 5 geostationary Earth Orbit (GEO) satellites, 5 inclined Geo Synchronous Orbit (IGSO) satellites, and 4 Medium Earth Orbit (MEO) satellites, which meet the requirements of serving the Asia Pacific region[17]. BDS-3 completed global networking in June 2020, including 3 GEO, 3 IGSO and 24 MEO satellites, to achieve global coverage, and provide global users with satellite navigation, positioning, speed measurement, time service, short message communications, interstellar enhancement, international search, emergency rescue and precision point positioning (PPP) services.

BDS-1 adopts an active positioning mode, while BDS-2 and BDS-3 provide both the active and passive positioning modes with a wider range of services. The BDS-2 is the first navigation satellite system that provides triple-frequency signals across the constellation. In addition to the test satellites and 3 GEO satellites, the rest of the BDS-3 satellites broadcast five open service signals. It abandons the B2I frequency based on BDS-2 but added three frequencies B2a, B2b and B1c [3,4]. A summary is

Editor-in-Charge: Dr. Xiaohong Zhang

given in Table 1.

Table 1: Frequencies of the different satellite navigation systems

	Band	Center frequency (MHz)
BDS-2	B1I	1561.098
	B2I	1207.140
	B3I	1268.520
BDS-3	B1I	1561.098
	B3I	1268.520
	B2a	1176.450
	B2b	1207.140
	B1C	1575.420
GPS	L1	1575.420
	L2	1227.600
	L5	1176.450

Since the first test satellite was launched in March 2015, plenty of scholars have analyzed the service performance of the BDS-3. Xie et al. [5] used the data from eleven IGMAS (International GNSS Monitoring And System) tracking stations to analyze the quality of the BDS-3 test satellites in terms of the BDS-3 multi-path effect, random noise and orbit error, which showed that the test satellite new atomic clocks performed better than the ones used by BDS-2. Wu et al. [6] studied the stability, accuracy and rate variation characteristics of the hydrogen atomic clock installed on BDS-3. The results showed that the performance of the hydrogen atomic clock on the satellites was similar to that on the ground, and the hydrogen atomic clock could provide stable timing and frequency standards. Li et al. [7] calculated the precise ephemeris of BDS-3 test satellites using the observation data from the Multi-GNSS Experiment (MGEX) and IGMAS tracking networks. By comparing the receiver clock error and the inter-frequency deviation between B1I and B3I, it confirmed that there was no obvious inter-system deviation on the same frequencies B1I and B3I between the BDS-2 and BDS-3 test satellites. Li et al. [8] attempted to improve the algorithm of the BDS-3 precise orbit and obtained pleasing results.

Up to now, most of the available studies about the signal quality, orbit products, constellation distribution, visibility, hardware performance, and so on of the BDS-3 satellites were conducted before the BDS-3 reached its global coverage [14-16]. However, the more research on the relative positioning performance of the full BDS-3 constellation and multi-frequency baselines with different lengths is beneficial to users, so are the in-depth studies in atmospheric error correction and ambiguity fixing. In this manuscript, a comprehensive performance analysis of BDS-3 and also compared with the BDS-2 and GPS in relative positioning are presented under the consideration of the essential relevant factors inclusive of the BDS-3 constellation, stability of multiple frequencies, solution convergence, positioning accuracy, etc. through baseline solutions at various lengths using our in-house developed software. The relative positioning algorithm was implemented under the condition of fully considering the influence of the relative positioning errors over the long baselines. Following this introduction, the mathematical model employed in this research is described in Section 2. In Section 3, we detail our experiments of the chosen baselines of different lengths using the BD3 multi-frequency observation data and discuss the stability, convergence speed and positioning accuracy of the BD3 multi-constellation and multi-frequency relative positioning from the results. Section 4 ends the manuscript with the conclusions and remarks.

2. Mathematical model

The single differenced observables between two ground stations have been employed herein relative positioning scheme. Because the residual errors of the ionosphere and troposphere delays are significant over the long baselines, their impact on the integer ambiguity resolution must be considered to reach high precise solutions. Hence, the pseudo-range and carrier phase observation equations are:

$$\Delta P_i = \Delta\rho + t + B_i + \Delta I_i + \Delta T + \Delta\varepsilon_i \quad (1)$$

$$\lambda_i \cdot \Delta\Phi_i = \Delta\rho + t + D_i - \lambda_i \cdot \Delta N_i - \Delta I_i + \Delta T + \Delta\varepsilon_{\Phi_i} \quad (2)$$

wherein Δ represents the single-differencing operator, P and Φ represent the pseudo-range carrier phase observations, respectively, ρ represents the geometrical distance from a receiver station to a satellite that is the function of the station

position coordinates, t represents the receiver's clock error, which is the clock error difference between the two receivers, B_i and D_i are the hardware delays associated with the pseudo-ranges and phases, respectively, which merge the hardware delays of two involved receivers and would be cancelled through double-differencing technique. With the short baselines, the atmospheric delays after the single differencing operation are normally eliminated or become negligible, which will not affect the integer ambiguities fixing process. With long baselines, such residual errors significantly affect carrier phase integer ambiguities fixing and position estimation by reducing the correlation of atmospheric delays between two GNSS stations. Such errors' effect could be greater than half of the carrier wavelength to cause the integer ambiguities fixing to fail. To successfully fix the integer ambiguities, it is paramount of considering the effect of the residual atmospheric delay errors. Therefore, the observation equations include the ionosphere and troposphere residuals together with the position parameters toward successfully fixing the ambiguities to integers.

The troposphere delay is commonly modeled after the Global Mapping Function (GMF) and the Relative Zenith Troposphere Delay (RZTD). The zenith troposphere delays of a reference station ***A*** (ZTD_A) and a second station ***B*** (ZTD_B) yield the following difference:

$$\begin{aligned}\Delta T_{AB} &= m_A \cdot ZTD_A - m_B \cdot ZTD_B \\ &= m_A \cdot \left(ZTD_A - ZTD_B\right) + (m_A - m_B) \cdot ZTD_B\end{aligned} \tag{3}$$

wherein m represents the mapping function of the troposphere delay error. When the distance between two stations is about 300km or shorter, with the common-visible satellites, this difference is small so that $(m_A - m_B) \cdot ZTD_B$ can be ignored. Then (3) is simplified to:

$$\Delta T_{AB} \approx m_A \cdot \left(ZTD_A - ZTD_B\right) = m_A \cdot RZTD \tag{4}$$

wherein $RZTD$ is the relative zenith troposphere delay error between two stations. In general, for a reference satellite ***k*** and another satellite ***s*** among the ***n*** satellites at the current epoch, the observation equations for three frequency carrier phase integer ambiguities, residual error of the relative zenith troposphere delays and residual ionosphere delay errors are as follows:

$$\begin{bmatrix} v_{\phi 1}^{sk} \\ v_{\phi 2}^{sk} \\ v_{\phi 3}^{sk} \\ v_{P1}^{sk} \\ v_{P2}^{sk} \\ v_{P3}^{sk} \end{bmatrix} = \begin{bmatrix} a^{sk} & m^{sk} & -b & -\lambda_1 \cdot b & 0 & 0 \\ a^{sk} & m^{sk} & -(f_1^2 / f_2^2) \cdot b & 0 & -\lambda_2 \cdot b & 0 \\ a^{sk} & m^{sk} & -\left(f_1^2 / f_3^2\right) \cdot b & 0 & 0 & -\lambda_3 \cdot b \\ a^{sk} & m^{sk} & b & 0 & 0 & 0 \\ a^{sk} & m^{sk} & (f_1^2 / f_2^2) \cdot b & 0 & 0 & 0 \\ a^{sk} & m^{sk} & \left(f_1^2 / f_3^2\right) \cdot b & 0 & 0 & 0 \end{bmatrix} \begin{bmatrix} X \\ RZTD \\ I_1^s \\ I_1^k \\ \Delta N_1^s \\ \Delta N_1^k \\ \Delta N_2^s \\ \Delta N_2^k \\ \Delta N_3^s \\ \Delta N_3^k \end{bmatrix} - \begin{bmatrix} L_{\phi 1}^s - L_{\phi 1}^k \\ L_{\phi 2}^s - L_{\phi 2}^k \\ L_{\phi 3}^s - L_{\phi 3}^k \\ L_{P1}^s - L_{P1}^k \\ L_{P2}^s - L_{P2}^k \\ L_{P3}^s - L_{P3}^k \end{bmatrix} \tag{5}$$

Among them, the upper sign represents the satellite number, $b = \begin{bmatrix} 1 & -1 \end{bmatrix}^T$, X is the position parameters after the linearization of the observation equation, is the vector of the position parameter coefficient, m is the coefficient of the station relative zenith troposphere, I is the Ionosphere delay error of B1, N_1、N_2、N_3 is the ambiguity vectors associated with the four carrier waves, $L_{\phi 1}$、$L_{\phi 2}$、$L_{\phi 3}$ is the carrier phase observations associated with the three carrier waves, L_{P1}、L_{P2}、L_{P3} are the pseudo-range observations.

With *n* commonly observed satellites at an epoch, *n*-1 double difference observations can be obtained by

projection, which can eliminate the clock error and hardware delays of the receiver, with which the integer ambiguity and the residual atmospheric delays are in the form of single differences between two stations. Single differences parameters are with respect to individual satellites. So, it is conducive to putting the constraints on the residual atmospheric delays and the reference satellite switching in the ambiguity resolution process into practice. In this paper, the reference ambiguity associated with a satellite possessing a higher elevation angle in the initial epoch is selected as the reference ambiguity and its value is approximated using the available pseudo-ranges at that epoch.

A well-known fact is that the ionosphere delay associated with a specific satellite is equal in size but with the opposite sign on the pseudo-range and carrier phase observations, while the troposphere delay is the same on both of them. Hence, the integration of the pseudo-ranges and carrier phases undoubtedly strengthens the constraint on the residual ionosphere and troposphere delay errors. The noise in a pseudo-range observation is very large in comparison with the one in a carrier phase observation. Empirically, these two observations are weighted according to the weighting ratio of 1:10000.

Due to the additional parameters for modeling the residual atmosphere errors, there will be too many unknown parameters which will weaken the estimability of the equation system and make it difficult to be solvable. To prevent the normal equation from being ill-conditioned and at the same time to strengthen the positioning solution, the change of the residual troposphere and ionosphere errors are considered as random walk process from time to time, which are corresponding to apply the prior constraints to their estimation process. The constraints based on the random walk process for the residual errors of the zenith troposphere delay and the ionosphere delay, respectively, are epoch wise as follows [12,13]:

$$RZTD(t_{k+1}) - RZTD(t_k) = w(t_k),\ w(t_k)\tilde{N}(0, q_T^2) \quad (6)$$

$$I(t_{k+1}) - I(t_k) = \psi(t_k),\ \psi(t_k)\tilde{N}(0, q_I^2) \quad (7)$$

wherein $w(t_k)$ and $\psi(t_k)$ are the changes of the zenith troposphere delay error and the ionosphere delay error from moment t_k to moment t_{k+1}, respectively, modeled as random walk process, q_T and q_I is the power spectral density of the corresponding residual troposphere and ionosphere delay errors. Indeed, the constraints in (6) and (7) are equivalent to that the change of the residual troposphere and ionosphere delay adopt the constraints of the random walk process from time to time.

The estimated residual atmospheric delays at the current epoch are transferred to the next epoch in the form of random constants, After the normal equation system is superimposed, the parameter eliminating method is applied to eliminate the atmospheric delay parameters of the current epoch and the atmospheric delay parameters of the next epoch are retained. The influence of the current epoch parameter information is cascaded to follow the normal equation to the next epoch. Refer to [18] for the specific detailed implementation. The principle of parameter elimination is applied to solve the following normal equation system:

$$\begin{cases} \mathrm{V=BX-L} \\ \begin{bmatrix} \mathrm{N}_{x_0x_0} & \mathrm{N}_{x_0x_1} & \mathrm{N}_{x_0x_2} \\ \mathrm{N}_{x_1x_0} & \mathrm{N}_{x_1x_1} & \mathrm{N}_{x_1x_2} \\ \mathrm{N}_{x_2x_0} & \mathrm{N}_{x_2x_1} & \mathrm{N}_{x_2x_2} \end{bmatrix} \begin{bmatrix} x_0 \\ x_1 \\ x_2 \end{bmatrix} = \begin{bmatrix} \mathrm{W}_0 \\ \mathrm{W}_1 \\ \mathrm{W}_2 \end{bmatrix} \end{cases} \quad (8)$$

with $N = B^T PB, \mathrm{W} = B^T PL$ and $X = [x_0 \quad x_1 \quad x_2]^T$, wherein x_0 and x_2 are the position and ambiguity parameters while x_1 is the atmospheric parameter vector, which is to be eliminated. From the second equation in (8), one can easily express x_1 as the function of x_0 and x_2:

$$x_1 = \mathrm{N}_{x_1x_1}^{-1}\left(\mathrm{W}_1 - \mathrm{N}_{x_1x_0}x_0 - \mathrm{N}_{x_1x_2}x_2\right) \quad (9)$$

Substituting (9) into the first and third equations of (8) yields:

$$\begin{bmatrix} N_{x_0x_0}-N_{x_0x_1}N_{x_1x_1}^{-1}N_{x_1x_0} & N_{x_0x_2}-N_{x_0x_1}N_{x_1x_1}^{-1}N_{x_1x_2} \\ N_{x_2x_0}-N_{x_2x_1}N_{x_1x_1}^{-1}N_{x_1x_0} & N_{x_2x_2}-N_{x_2x_1}N_{x_1x_1}^{-1}N_{x_1x_2} \end{bmatrix} \begin{bmatrix} x_0 \\ x_2 \end{bmatrix} = \begin{bmatrix} W_0-N_{x_0x_1}N_{x_1x_1}^{-1}W_1 \\ W_2-N_{x_2x_1}N_{x_1x_1}^{-1}W_1 \end{bmatrix} \quad (10)$$

which does not contain x_1 any more, although its information is preserved. (9) and (10) are equivalent in terms of x_0 and x_2.

After the elimination of the atmospheric parameters, the remaining unknown parameters, for example, the coordinates and ambiguities can directly be solved, The floated ambiguities solution is further processed using the Least-square AMBiguity Decorrelation Adjustment (LAMBDA) algorithm, which attempts to fix the floated ambiguities to integers. Then, the coordinates are estimated again under the consideration of the fixed integer ambiguities as known constants. In this way, the estimated coordinates achieved the best possible accuracy. For purpose of analyzing the estimation results handily, the baseline vector (i.e., the ECEF incremental coordinates) between two stations need to be converted into their E, N and U components relative to the base station. Then one can acquire the position discrepancies of the second station (equivalent to the baseline) as time series.

3、 Experimental analysis

To evaluate the positioning performance of BDS-2, BDS-3 and GPS systems, six baselines of different lengths were selected for experiments. The convergence speed and positioning accuracy of the experimental results were statistically analysed in this research. The location distribution of the test sites is shown in Figure 1. Table 2 overviews the selected baselines.

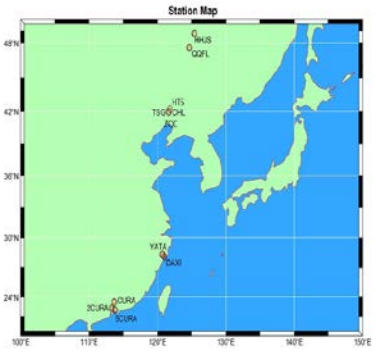

Figure 1: Site distribution map

Table2: Overview of the selected baselines

Baseline	Length (km)	Start Time (UTC)	Length (min)	Receiver	The station location
TSG-CHL	0.6	00:00:00	360	Sino K708	Liaoning
HTS-ZQC	15	00:17:00	140	Sino K708	Liaoning
YATA-DAXI	37	06:00:00	360	Trimble Maxwell	Zhejiang
2CURA-5CURA	54	00:00:00	600	Sino K708	Guangzhou
CURA-5CURA	93	00:00:00	600	Sino K708	Guangzhou
HHJS-QQFL	147	00:00:00	600	Unicore ub4b0	Heilong-jiang

The data associated with the selected baselines were processed for BDS-2, BDS-3, GPS individually and also jointly for multi-constellation. The satellite cut-off elevation angle was set to 15 degrees and the sampling rate was 1 Hz. The baselines of 0.6 km, 15km and 37 km were divided into small stretches every ten minutes, as the other baselines of 54 km, 90 km and 147 km were divided into hourly stretches to result in relative positioning solutions. In data processing, BDS-2 used B1I, B2I and B3I three frequencies, BDS3 used B1I, B3I, B1c and B2a four frequencies and GPS used L1 and L2 two frequencies.

As the atmospheric delay errors increasing with the length of baselines, it is a challenge how to deal with them in such applications. Without appropriately compensating the atmospheric errors, the long baseline relative positioning would become very difficult to fix the ambiguities to integers. In this studying, the changes of the residual atmospheric delays associated with the long baselines were characterized as a random walk process [12].

The troposphere delay is relatively stable for the whole day. So, the tense random walk constraint has a pretty effect on it. When the ionosphere delay is relatively stable, the tense constraint effect on ionosphere delay is better. However, if the ionosphere

change is unstable, for example, when the light is strong, the ionosphere change is intense and one gives the ionosphere delay a loose constraint, it is more conducive to the estimation of the unknown parameters. Figure 2 shows the ionosphere error of the four satellites C21, C34, C39 and C44 of BDS-3 with the 93 km long baseline.

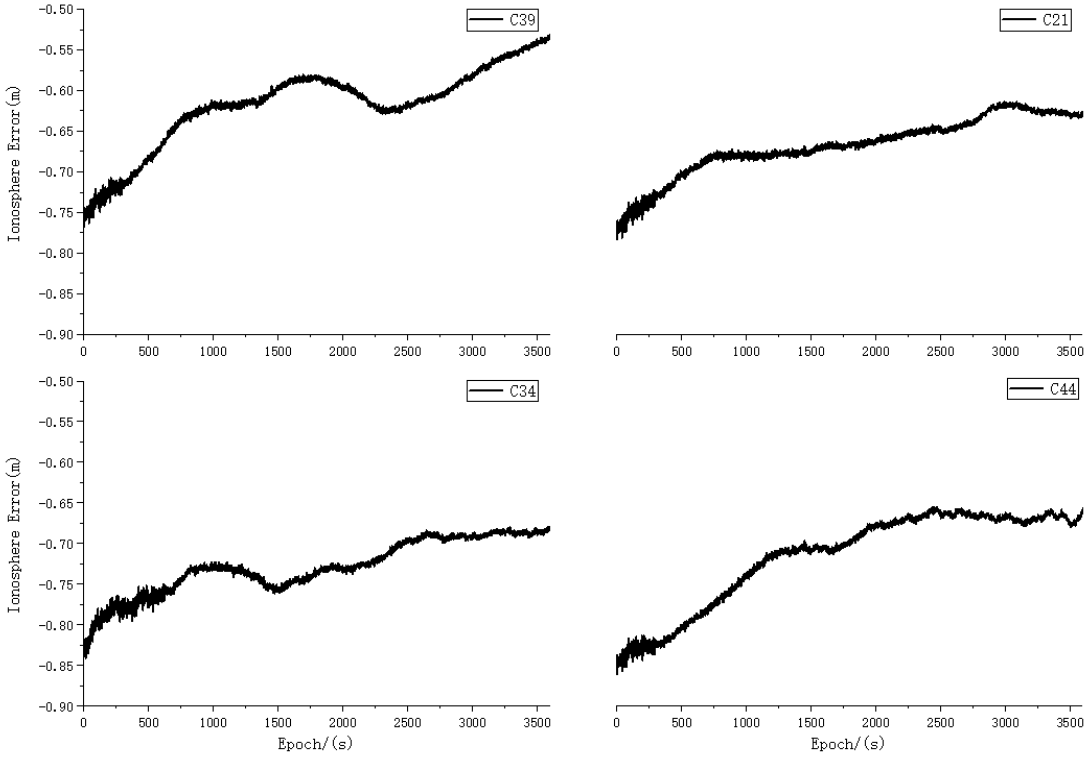

Figure 2: 93km single-differenced ionosphere error

As can be seen from Figure 2, the change of the ionosphere delays was greater than the half wavelength of the carrier waves. Mixed with other effects together such as orbit error, multipath effect, observation noise, it would make the ambiguities fixing very difficult. Besides, if the residual atmospheric error was used as a parameter to estimate, the atmospheric error can be separated, and the integer ambiguity can be fixed more easily. Figure 3 shows the convergence process of the floated ambiguities with the 93km long baseline.

In the integer ambiguity fixing process, the residual atmospheric errors and other errors were either constrained or approach eliminated to reduce the overall error effect less than the half wavelength of the carrier wave, so that the ambiguities can be fixed easily. From Figure 3, the estimated float ambiguities soon converged close to the accurate integer ambiguities, then the LAMBDA algorithm was applied for an integer ambiguity resolution. The amount of computation was adequate and the success rate is high indeed.

As the selected baselines were located within China, the number of the visible GEO and IGSO satellites of the Beidou navigation system was high. From Figure. 4(d, e and f), it can be seen that, in the low latitude area, a maximum of 13 and a minimum of 8 BDS-2 satellites were observed. The number of the common- visible satellites was significantly higher than the ones from BDS-3 and GPS. Because the main coverage of the BDS-2 satellites is from the latitude of 30 degrees north to 30 degrees south and the longitude of 90 degrees east to 150 degrees range [9], with the rising of the latitude, the number of the common-visible BDS-2 satellites was decreased slightly. The BDS-3 and GPS systems are global satellite navigation systems, are mainly composed of MEO orbit satellites. The total number of the BDS-3 satellites was approximately equivalent to the number

of GPS satellites. But their satellite orbits are not as reasonable as GPS satellites, even in China the number of the common-visible satellites was just approximately equal to the number of visible GPS satellites. The number of visible BDS-3 or GPS satellites was roughly about eight.

The data for the short baselines were divided into short stretches with 600 epochs. The 0.6km and 15km long baselines (Fig. 4 and Fig. 5) were similar to the 37km long baseline (Fig. 6) because the baselines are short, the receiver clock error, satellite clock error, hardware delay error and atmospheric delay error are highly correlated and also can be eliminated approximately through the double differencing process. As can be seen from Fig. 4, Fig. 5 and Fig. 6, the BDS-2, BDS-3 and GPS systems could fix the ambiguities in the first epoch. Therefore, they have the same convergence speed.

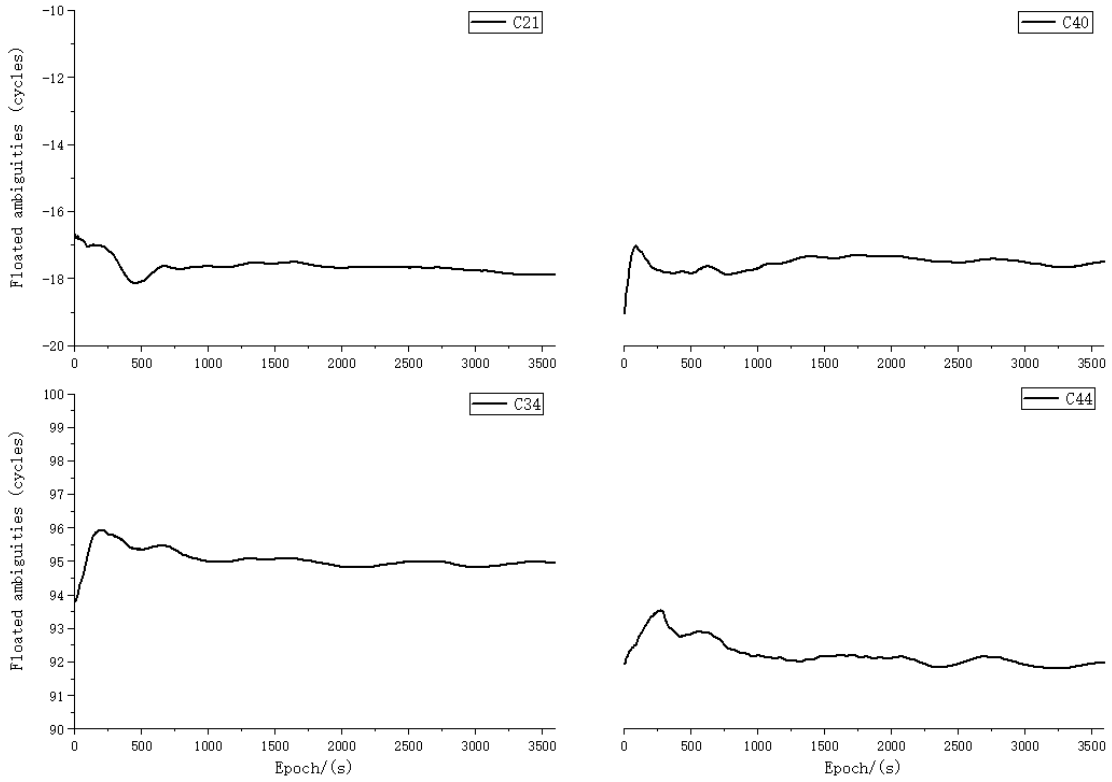

Figure3: The floated ambiguities with the 93km long baseline

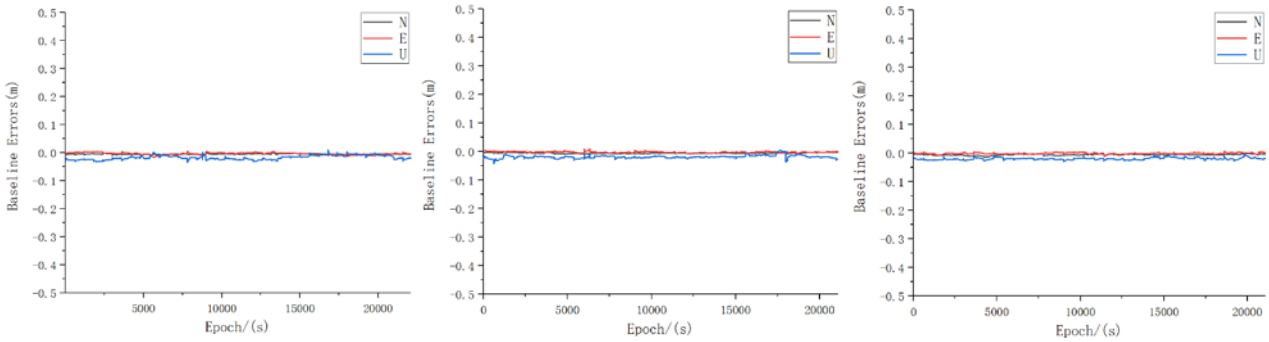

(a): BDS-2 baseline errors; (b): BDS-3 baseline errors (c): GPS baseline errors

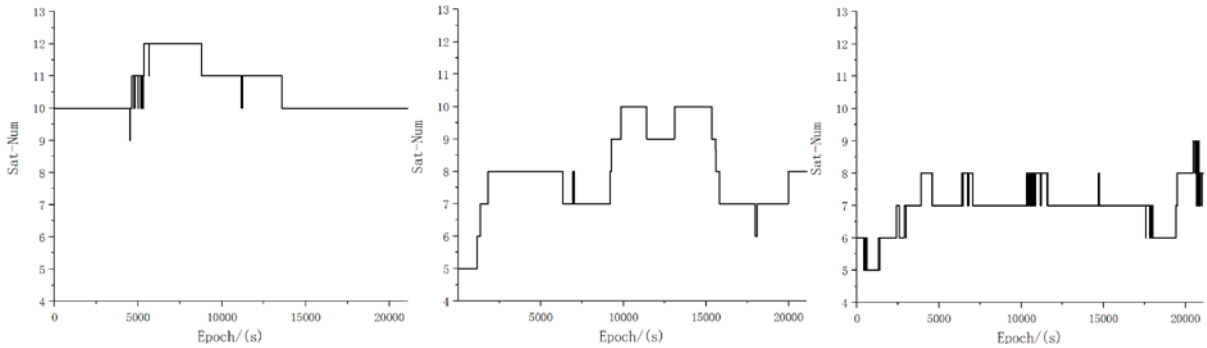

(d): Number of BDS-2 satellites (e): Number of BDS-3 satellites (f): Number of GPS satellites

Figure 4: The 0.6km long baseline performance comparison

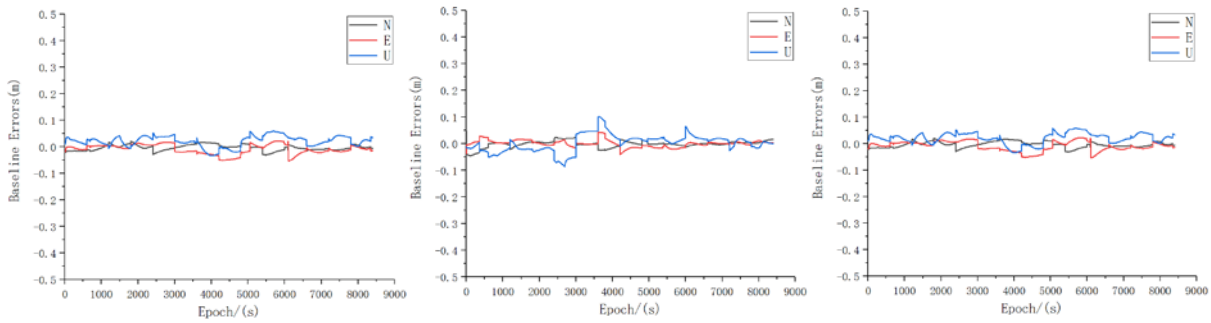

(a): BDS-2 baseline errors (b): BDS-3 baseline errors (c): GPS baseline errors

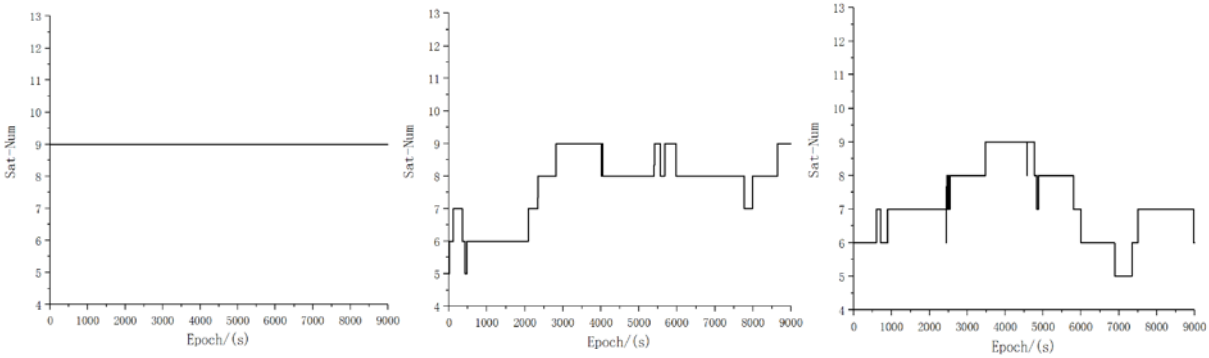

(d): Number of BDS-2 satellites (e): Number of BDS-3 satellites (f): Number of GPS satellites

Figure 5: The 15km long baseline performance comparison

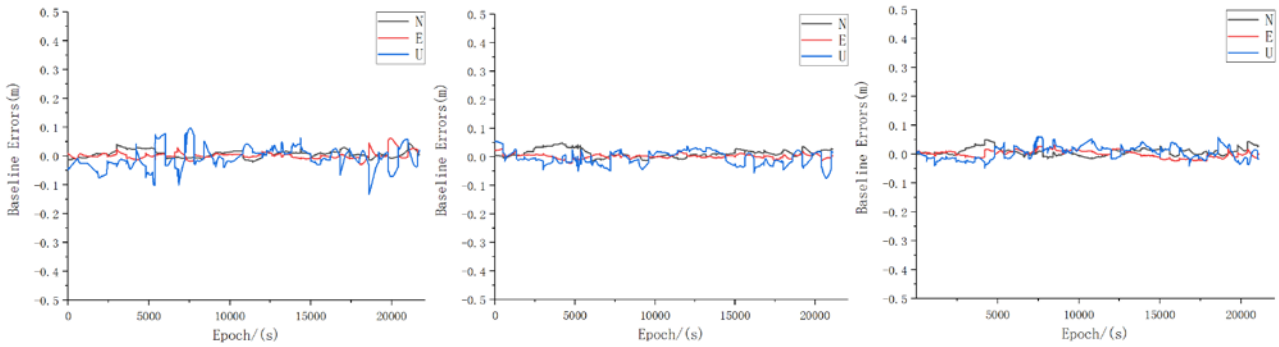

(a): BDS-2 baseline errors (b): BDS-3 baseline errors (c): GPS baseline errors

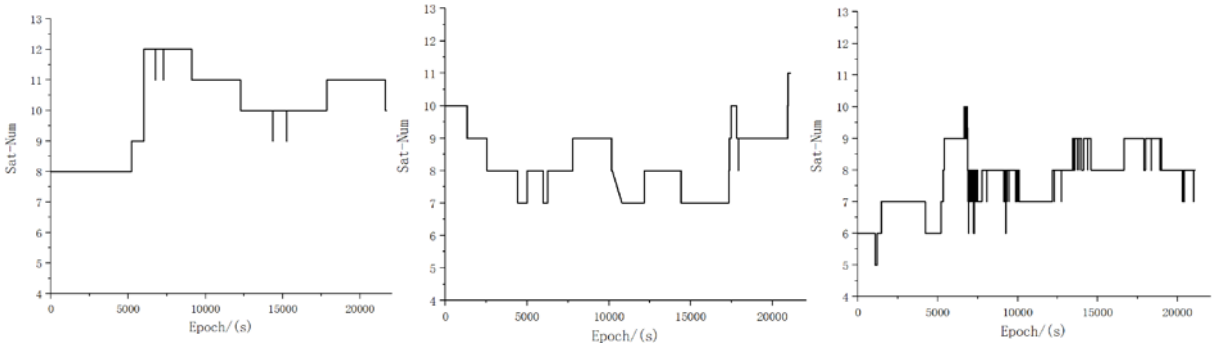

(d): Number of BDS-2 satellites (e): Number of BDS-3 satellites (f): Number of GPS satellites

Figure 6: The 37km long baseline performance comparison

From the analysis given in Fig. 7, Fig. 8 and Fig. 9 for the 54km, 93km and 147km long baselines, respectively, it can be seen that the solution convergence speed had a strong correlation with the number of common-visible satellites. The number of satellites changes more stable period convergence speed was faster, otherwise, convergence speed and positioning accuracy were reduced.

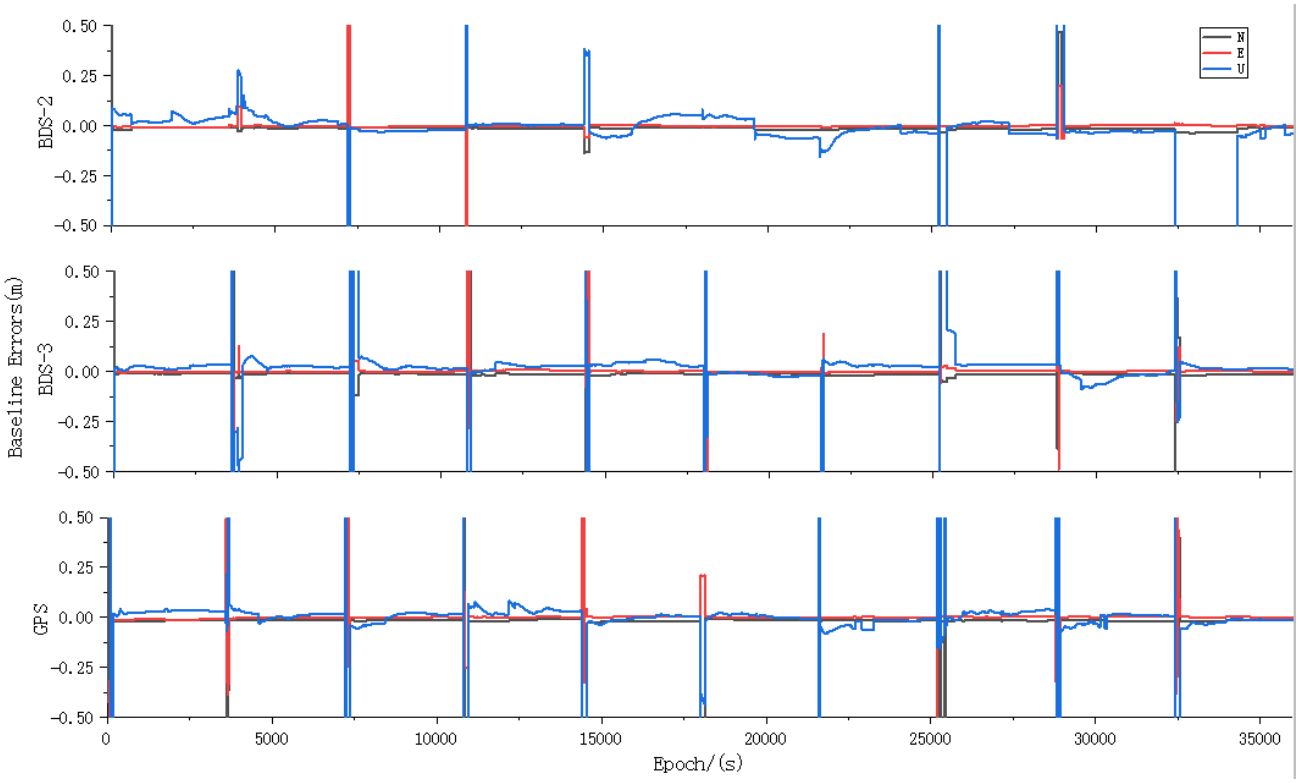

(a): baseline errors

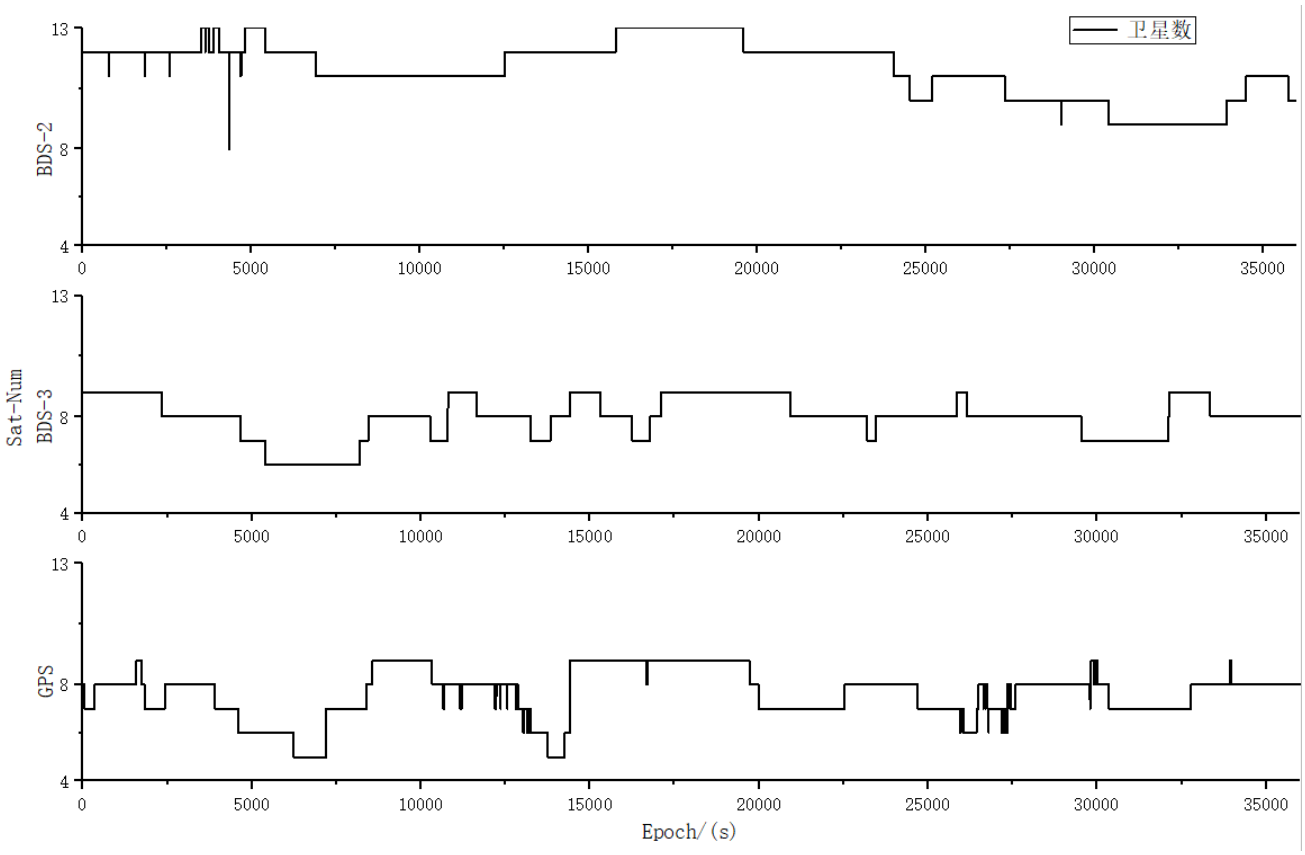

(b): Number of satellites

Figure 7: The 54km long baseline performance comparison

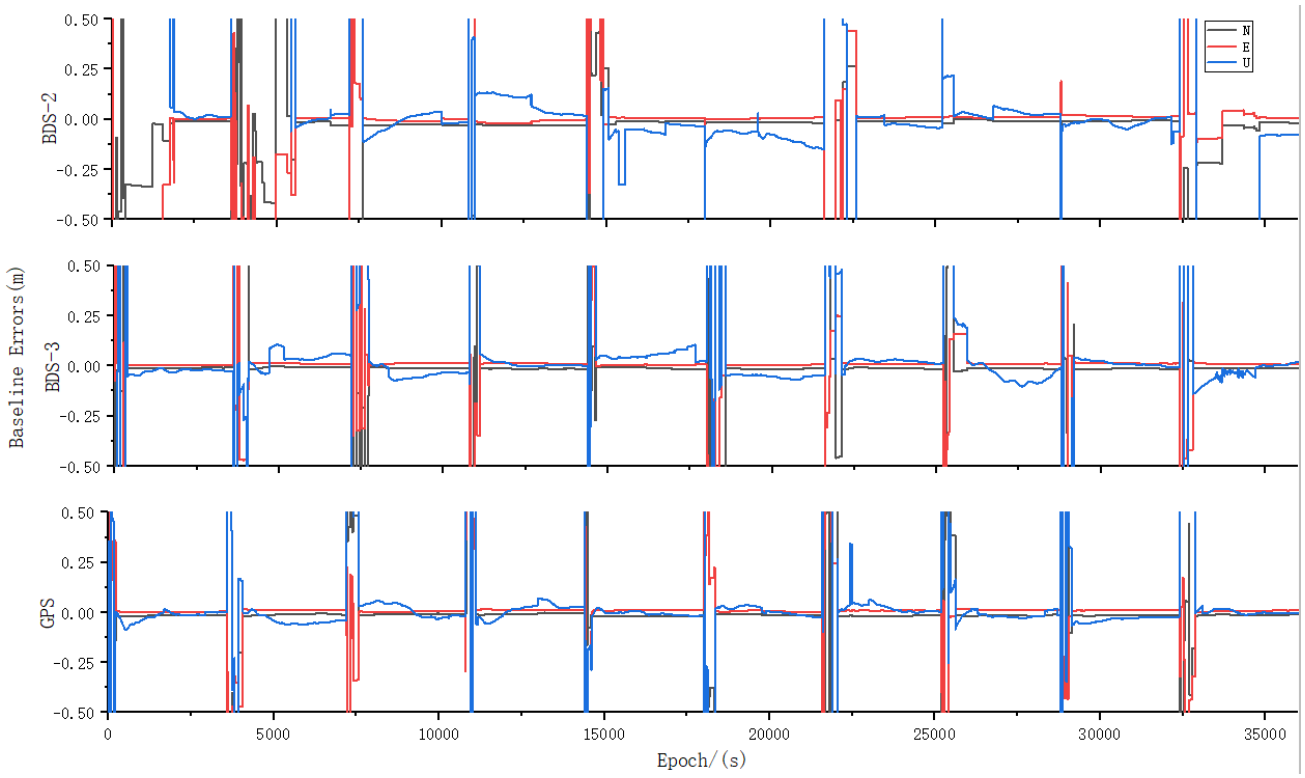

(a): baseline errors

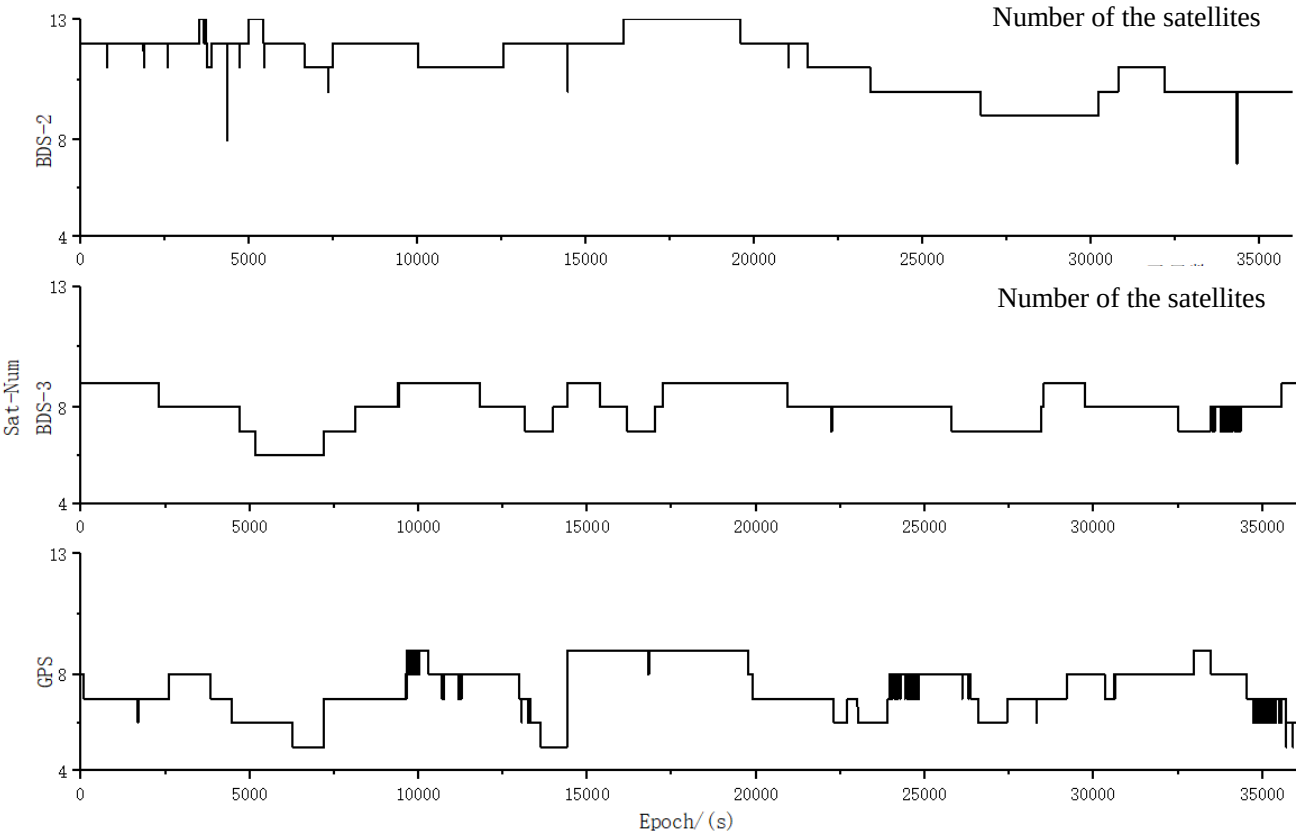

(b): Number of satellites

Figure 8: The 93km long baseline performance comparison

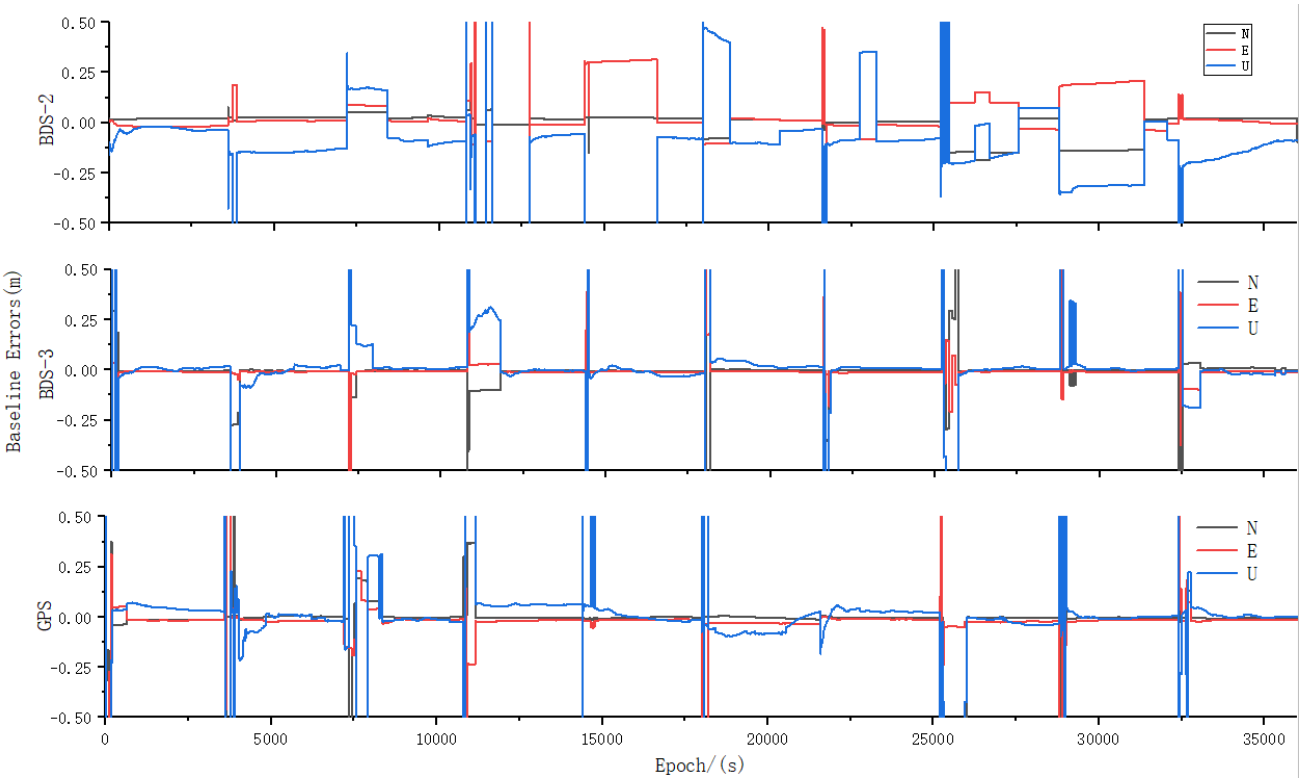

(a): BDS-2 baseline errors

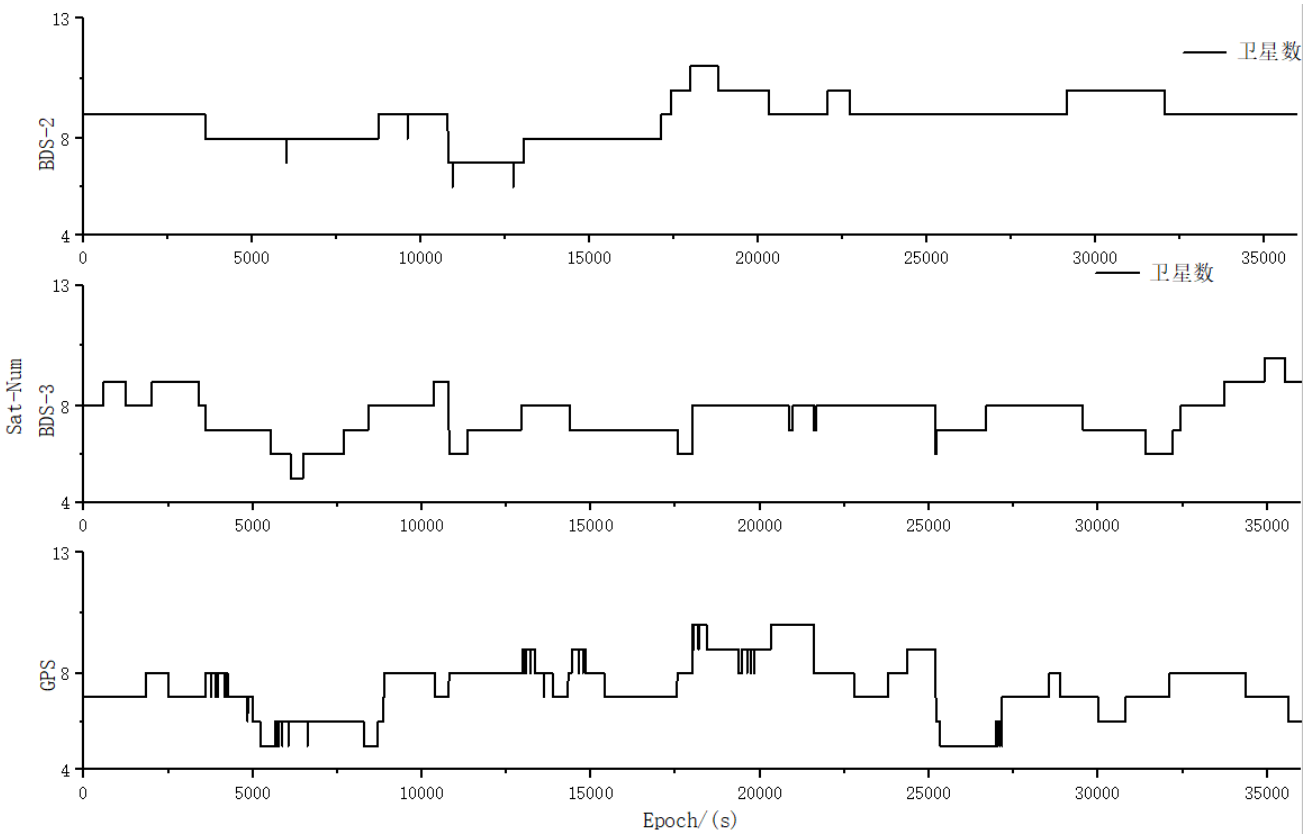

(b): Number of satellites

Figure 9: The 147km long baseline performance Comparison

Table 3 gives the statistics of the convergence speeds according to the time when that baseline accuracy reaches the centimeter-level for the 54km, 93km and 147km long baselines, whose average convergence times were also plotted in Fig. 10. The short baselines of 0.6km, 15km and 37km can be fixed in a single epoch right away, so there is no need to list them in the table.

Table 3: Convergence time statistics

Baseline / Epochs	54km			93km			147km		
(System)	BDS-2	BDS-3	GPS	BDS-2	BDS-3	GPS	BDS-2	BDS-3	GPS
1	23	10	169	1764	386	218	135	210	186
3600	494	353	112	1955	478	469	2107	138	230
7200	71	292	434	564	533	1560	263	288	193
10800	43	99	141	216	322	310	633	405	367
14400	167	117	161	676	239	232	1924	90	368
18000	339	107	146	277	574	341	2396	158	194
21600	2	28	31	987	517	755	816	236	69
25200	270	499	242	339	728	461	1649	496	809
28800	318	45	136	5	374	425	2359	310	221
32400	1898	149	155	2416	697	332	2566	652	384
Average	362.5	169.9	172.7	919.9	484.8	510.3	1485	298.3	302.1

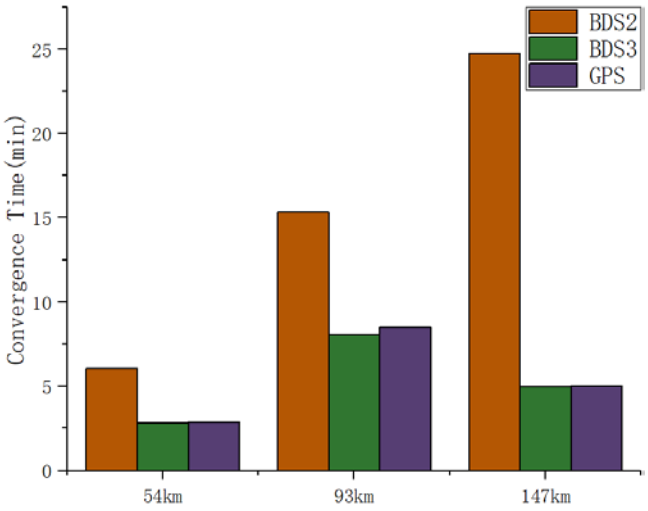

Figure 10: The average convergence time

Table 4: Statistics of the baseline errors

Direction / Length	System	N[m]	E[m]	U[m]
	BDS-2	0.017722	0.006063	0.046523
147KM	BDS-3	0.013104	0.008905	0.022591
	GPS	0.012631	0.009452	0.01736
	BDS-2	0.012235	0.007075	0.040118
93KM	BDS-3	0.015987	0.011874	0.017434
	GPS	0.012914	0.009377	0.018792
	BDS-2	0.01346	0.003047	0.03409
54KM	BDS-3	0.01335	0.002329	0.022449
	GPS	0.014991	0.003257	0.019073
	BDS-2	0.012019	0.006684	0.025455
37KM	BDS-3	0.013819	0.006137	0.018835
	GPS	0.010874	0.009495	0.018477
	BDS-2	0.009026	0.014461	0.02332
15KM	BDS-3	0.007294	0.008232	0.019878
	GPS	0.009398	0.011895	0.01793
	BDS-2	0.005011	0.004152	0.017102
0KM	BDS-3	0.004963	0.001826	0.018226
	GPS	0.005542	0.001498	0.01952

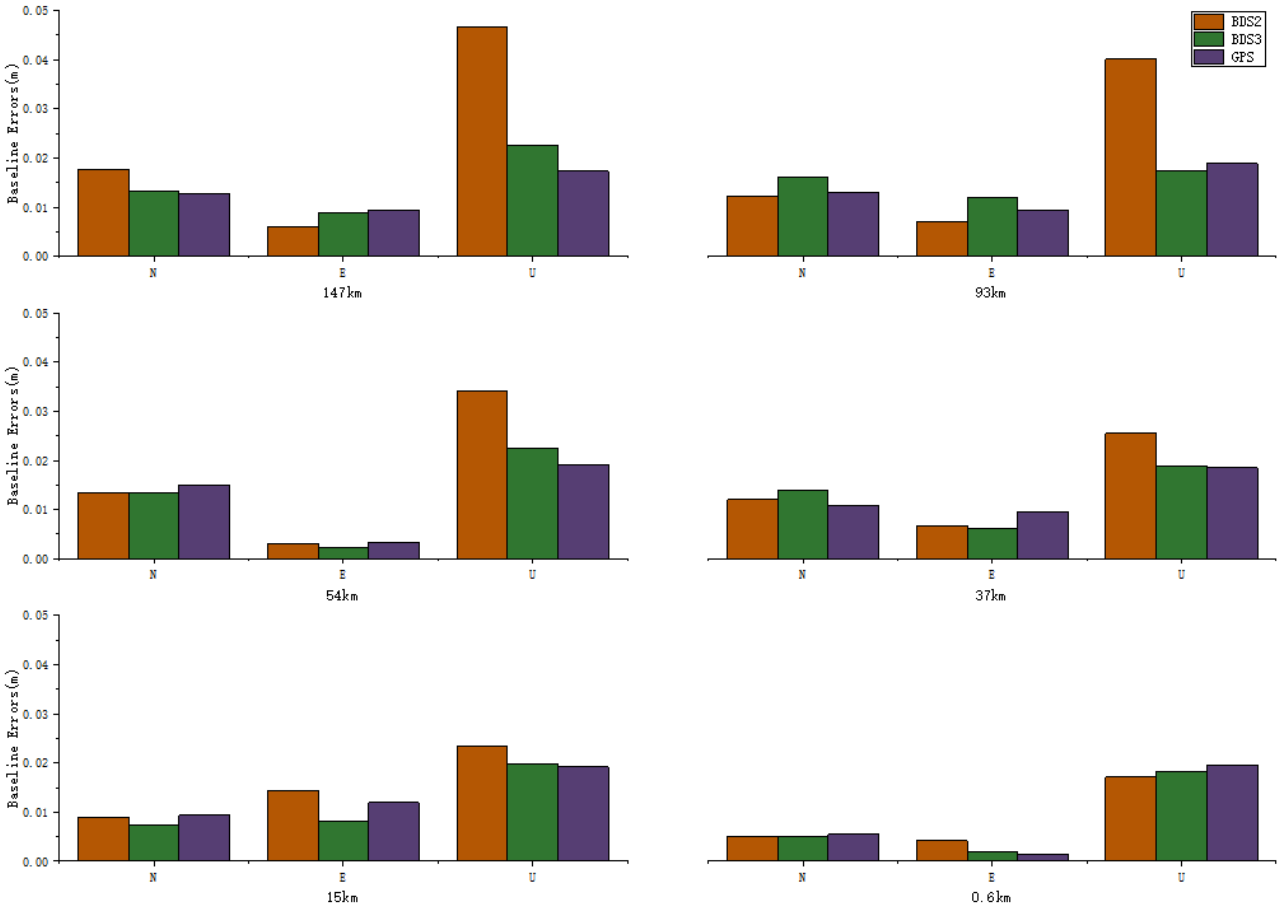

Figure 11: Chart of the baseline errors

Table 4 summarizes the average errors of six baselines resulted from each of the three systems: BDS-2, BDS-3 and GPS.

In Fig. 11, the baseline errors resulted from each of the three systems for each of the selected baselines were plotted. For the 0.6km short baseline, the solution converged in a single epoch. The average accuracy of the baseline solution was similar with each of the three systems. Although with the solutions of the 15km and 37km long baselines, the BDS-2 convergence speed was the same as the BDS-3 and GPS systems so that the ambiguities could be fixed in a single epoch. However, the residual error leads to baseline accuracy being lower than the accuracy of the 0.6km long baseline. The 54km, 93km and 147km long baselines, whether it comes to their convergence speeds or final baseline accuracy, the BDS-2 performed the worst. Although the number of BDS-2 satellites was the highest, the positioning performance was also unsatisfactory. The observed BDS-2 satellites were mostly the GEO and IGSO satellites on the 36,000km high orbits. Therefore, the satellites run slowly with a longer operating cycle. The composition of the constellation geometry is not as good as the MEO satellites. The BDS-2 is not conducive to the continuous calculation of observation data, so the solution took longer to go convergent. The convergence speed with the BDS-2 would be accelerated with the increase of the number of the MEO satellites because the MEO satellites have their lower orbit height, which means a high running speed. When enough satellites of MEO are tracked, the satellite constellation geometry will change quickly. Accordingly, the convergence speed of the baseline solution with the BDS-2 system is improved.

According to the statistics of the accuracy results, with the increase of the baseline length, the convergence time of ambiguities resolution also increased, and the solution accuracy was reduced. With the long baseline solutions even if the atmospheric delays were constrained, the influence of residual atmospheric delays could not be wholly compensated. Hence, the residual atmospheric errors

would slow down the convergence of the ambiguities resolution. When the ambiguities are accurately fixed, the residual atmospheric delay errors will be absorbed by the baseline parameters, which would decrease the baseline solution accuracy. The baseline error in the U direction is the largest, which is 1.5 times of error in the N and E directions in general. The reason for this is that the residual errors of satellite orbits and troposphere delays would have a great influence on the U direction.

The BDS-3 system is mainly composed of the MEO satellites, which is geometrically favorable for continuous calculation. The BDS-3 satellites broadcast five frequency signals and have strong signal anti-noise ability. However, the ephemeris and related correction models with the BDS-3 satellites are not as good as the GPS. As can be seen from the solution error charts and the average convergence speed charts, the BDS-3 baseline accuracy is slightly worse than the GPS solutions, but BDS-3 convergence speeds were faster than the GPS.

4、 Conclusion

In this paper, the performance comparison of the relative positioning using three systems of BDS-2, BDS-3 and GPS was conducted. With short baselines as well known, the ionosphere and troposphere errors are highly correlated between stations and could be approximately eliminated through the between station differencing technique. The integer ambiguities resolution could be achieved in a single epoch with any of BDS-2, BDS-3 and GPS. With the long baseline relative positioning, because the atmospheric delays correlation becomes decreases between stations by degrees, the random walk constraint was introduced into the measurement model. Through the analysis of the atmospheric delay errors and the convergency of the floating ambiguities resolution, we discovered that the ambiguities with the BDS-3 satellites converged faster under the constraints on the residual atmospheric delays. The statistics of the results have found that the convergence speed with BDS-3 was twice as fast as the one with BDS-2. BDS-3 average convergence speed was also faster than GPS, which has increased by about 2.7%.

In comparison with BDS-2, BDS-3 has greatly improved the quality of its satellite orbits, atomic clocks, signal anti-noise ability, estimates of the frequency biases, broadening coverage, etc. So, its positioning performance has also achieved great ascension. The BDS-3 positioning accuracy in relative positioning has been improved by about 40% compared with BDS-2, but 7% lower than GPS.

The BDS-3 reached global coverage, compared with BDS-2, it has greatly improved in every aspect, but its positioning performance is still not as stable as GPS. At present, many models and algorithms for BDS-3 were adapted from GPS, which may not perfectly suitable for BDS-3. Indeed, BDS-3 provides us with many advantages over the others, e.g. GPS while it broadcasts five open frequency signals, uses three different satellite orbits, has the full constellation inter-satellite link, etc. So, there is still much space to improve the relevant models and algorithms when working on BDS-3 for high precision positioning applications

References

[1] YANG, Yuanxi (2010): Progress, Contribution and Challenges of compass-BeiDou Satellite Navigation System, ActaGeodaetica et Cartographica Sinica, 2010, 39(1): 1-6.

[2] YANG, Yuanxi; LI, Jinlong; XU, Junyi, et al (2011): Contribution of the Compass Satellite Navigation System to Global PNTUsers[J], Chinese Science Bulletin, 2011, 56(26): 2813-2819.

[3] China Satellite Navigation Office (2018): BeiDou Navigation Satellite System Open Service Performance Standard, Version 3.0, [EB/OL], 2018-12-27.

[4] China Satellite Navigation Office (2019): BeiDou Navigation Satellite System Signal In Space Interface Control Document Open Service Signal B1I, Version 3.0, [EB/0L], 2019-02-27.

[5] Xie, Xin; Geng, Tao; Zhao, Qile; Liu, Jingnan and Wang, Bin (2017): Performance of BDS-3: Measurement Quality Analysis, Precise Orbit and Clock Determination [J], Multidisciplinary Digital Publishing Institute,2017,17(6).

[6] Wu, Ziqian; Zhou, Shanshi; Hu, Xiaogong; et al (2018): Performance of the BDS-3 experimental satellite passive hydrogen maser [J], GPS

Solutions, 2018, 22(2).

[7] Li, Xingxing; Yuan, Yongqiang; Zhu, Yiting; et al (2019): Precise orbit determination for BDS-3 experimental satellites using iGMAS and MGEX tracking networks [J], Journal of Geodesy, 2019, 93(1):103-117.

[8] Li, Xingxing; Yuan,Yongqiang; Zhu, Yiting ; et al (2020): Improving BDS-3 precise orbit determination for medium earth orbit satellites [J], GPS Solutions: The Journal of Global Navigation Satellite Systems, 2020, 24(1).

[9] Cui, Haomeng; Wang, Jiexian; Wang, Minghua; et al (2020): Service Performance of BDS-3 by Satellite Distribution Probability [J], Geomatics and Information Science of Wuhan University,2020.

[10] Yao, Yibin; Zhao, Qingzhi (2016); A method to improve the utilization of GNSS observation for water vapor tomography [J], Annales Geophysicae, 2016, 34(1):143-152.

[11] Fan, Haopeng; Sun, Zhongmiao; Zhang, Liping; et al (2020): A Two-step Estimation Method of Troposphere Delay with Consideration of Mapping Function Errors [J], Journal of Geodesy and Geoinformation Science, 2020, 3(1):76-84.

[12] Tang, Weiming; Liu, Wenjian; Zou, Xuan; et al (2016): Improved ambiguity resolution for URTK with dynamic atmosphere constraints [J], Journal of Geodesy, 2016, 90(12):1359-1369.

[13] Zhang, Xiaohong; Ren, Xiaodong; Wu，Fengbo; et al (2019): Short-term Prediction of Ionospheric TEC Based on ARIMA Model [J], Journal of Geodesy and Geoinformation Science, 2019, 2(1):9-16.

[14] Li, Min; Yuan, Yunbin (2021); Estimation and Analysis of BDS-2 and BDS-3 Differential Code Biases and Global Ionospheric Maps Using BDS Observations [J], Remote Sensing, 2021, 13(3).

[15] Qin,Weijin; Ge, Yulong; Zhang, Zhe; et al (2020): Accounting BDS-3–BDS-2 inter-system biases for precise time transfer [J], Measurement, 2020, 156.

[16] Gao, Yueling; Hu, Xiaogong; Chen, Jinping; et al (2019): Initial analysis of the BDS satellite autonomous integrity monitoring capability [J], GPS Solutions, 2019, 23(2).

[17] China Satellite Navigation Office (2019): Development of the BeiDou Navigation Satellite System, Version 4.0, [EB/OL], 2019-12-27.

[18] Ge, Maorong; Liu, Jingnan (1996): The Estimation Methods For Tropospheric Delays in Global Positioning System [J], ActaGeodaetica et Cartographica Sinica, 1996(04):46-52.

Authors

Huizhong Zhu is an Associate Professor of School of Surveying and Geographic Science of Liaoning Technical University. He obtained his PhD from Wuhan University in 2012. His research is focused on high-precision GNSS positioning and data processing and has authored and coauthored 87 peer-reviewed papers.

Jingfa Zhang is a MEng student of School of Surveying and Geographic Science of Liaoning Technical University. His research is focused on high-precision GNSS positioning and data processing.

Jun Li is a PhD student of School of Surveying and Geographic Science of Liaoning Technical University. His research is focused on high-precision GNSS positioning and data processing

Qi Xu is a MEng student of School of Surveying and Geographic Science of Liaoning Technical University. His research is focused on high-precision GNSS

positioning and data processing

Yangyang Lu is a MEng student of School of Surveying and Geographic Science of Liaoning Technical University. His research is focused on high-precision GNSS positioning and data processing

Aigong Xu is Dean of School of Surveying and Geographic Science of Liaoning Technical University. He obtained his PhD from Wuhan University in 1998. His research is focused on high-precision GNSS positioning and data processing and has authored and coauthored 210 peer-reviewed papers.